NUREG/CR-0460

DEVELOPMENT OF HIGH-SENSITIVITY ULTRASONIC TECHNIQUES FOR IN-SERVICE INSPECTION OF NUCLEAR REACTORS

Annual Report

October 1, 1976 — September 30, 1977

M. Linzer
D. Dietz S.I. Parks

National Bureau of Standards

Prepared for
U.S. Nuclear Regulatory Commission

Available from
National Technical Information Service
Springfield, Virginia 22161
Price: Printed Copy $4.50 ; Microfiche $3.00

The price of this document for requesters outside of the North American Continent can be obtained from the National Technical Information Service.

NUREG/CR-0460

DEVELOPMENT OF HIGH-SENSITIVITY ULTRASONIC TECHNIQUES FOR IN-SERVICE INSPECTION OF NUCLEAR REACTORS

Annual Report
October 1, 1976 — September 30, 1977

M. Linzer, Principal Investigator
D. Dietz S.I. Parks

Manuscript Completed: May 1978
Date Published: October 1978

Institute for Materials Research
National Bureau of Standards
Washington, D.C. 20234

Prepared for the
Division of Reactor Safety Research
Office of Nuclear Regulatory Research
U.S. Nuclear Regulatory Commission
FIN No. B5680

ABSTRACT

During the period covered by this report, an ultrasensitive ultrasonic system, incorporating real-time signal averaging, pulse compression, dynamic focusing and transducer matching, has been developed. The system was shown to be capable of penetrating highly-attenuating material, such as austenitic steel, and of detecting reflections in the presence of strong background signals due to grain scattering.

I. INTRODUCTION

Techniques which improve the signal-to-random-noise ratio of ultrasonic signals may be used to locate minute flaws, presently undetectable, which might grow to larger size during service; to remotely inspect regions which have limited access, either because of the physical constraints of the reactor design or because of radiation hazards; and to locate flaws which are embedded within or accessed through highly-attenuating material, such as coarse-grain austenitic steel.

An ultrasensitive ultrasound inspection system with order of magnitude improvement in signal-to-random-noise ratio over conventional devices has been developed. Sensitivity enhancement is achieved by increasing the energy transferred to and from the material in the region of interest. Major features of the system include the use of repetitive pulses combined with signal averaging, the use of time-coded expanded pulses, and dynamic focusing. A real-time A-scan averager has been constructed which is capable of a S/N improvement of 1000:1 over single-scan measurement in about one minute of averaging. Pulse expansion and compression are accomplished by means of chirp radar techniques, with a compression ratio of 30:1 and compressed pulse width of 0.20 μs (~0.6 mm range resolution in the case of steel) demonstrated to date. For dynamic focusing, a unique signal processing scheme based on the use of an "expanding aperture" annular-array transducer is employed. Other high-sensitivity techniques which have been investigated include high-power insonification and matching of the acoustic impedances of the transducer and material.

The system was used to penetrate highly-attenuating material, such as austenitic steel. Furthermore, the dynamic focusing system was shown to be capable of reducing coherent background noise arising from grain scattering.

II. RESULTS

1. Signal Averaging

A high-speed signal averaging system, supported by the NBS program in NDE, has been completed. The system is capable of real-time (unbuffered) averaging at 50 MHz rates. Major features include 4K 24 bit words, 12.5 KHz maximum repetition rate, computer interface, 6-digit cursor readout of signal amplitude, region of interest expand (up to a factor of 16), 3-digit settability of sample rate, internal/external trigger, internal delay, segmented memory capability (full, halves, quadrants, octants), plug-in ADC's (4 bit, 50 MHz; 8 bit, 20 MHz), display normalization and semi-real time display at high frequencies. The sensitivity-enhancement capability of the averager was demonstrated on a number of highly-attenuating materials, including centrifugally-cast stainless steel, a fiber composite (Figure 1a), teflon (Figure 1b) and austenitic steel (Figure 1c). Flaw detection in the case of the austenitic steel sample was limited by the coherent background signals arising from grain scattering within the material.

The inability of signal averaging to reduce "structural" noise was demonstrated in a series of experiments on a 6" x 6" section of 24" diameter, 2" thick centrifugally-cast stainless steel tubing. The tubing was ultrasonically tested in reflection at 2.25, 5 and 10 MHz frequencies. Penetration through both the 6" and 2" paths was attempted. In some regions, backwall reflections could be seen, even without signal averaging, to frequencies as great as 10 MHz, while in other regions, no backwall reflection could be obtained at frequencies as low as 2.25 MHz, even with signal averaging. A two-transducer transmission measurement was then made through the 6" path. (Figure 2) Results of this study is shown in Figure 3.

(a)

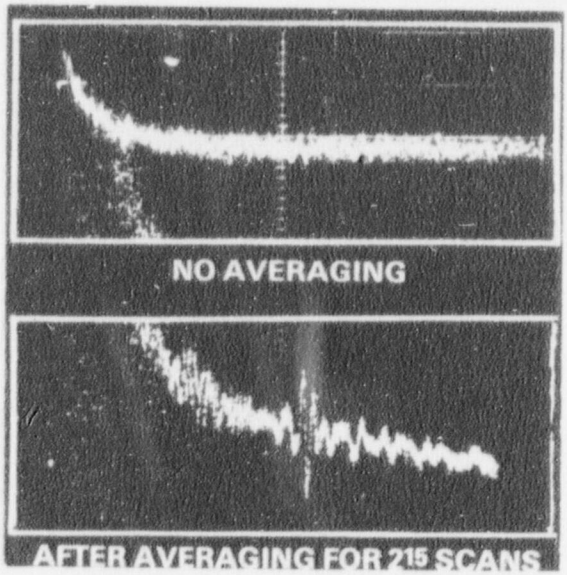

(b)

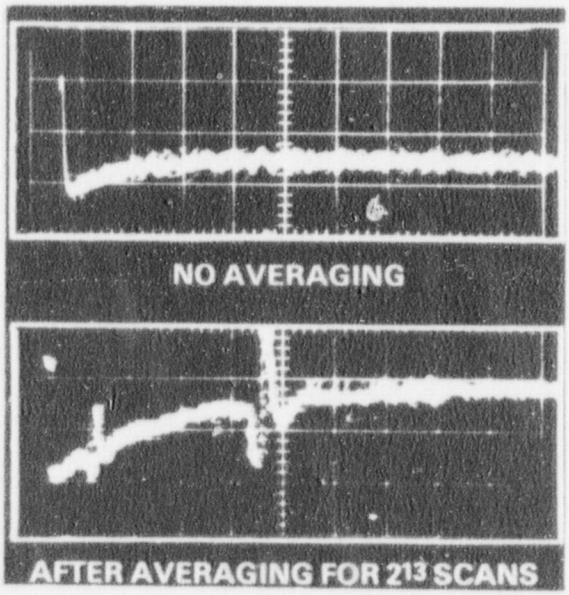

(c)

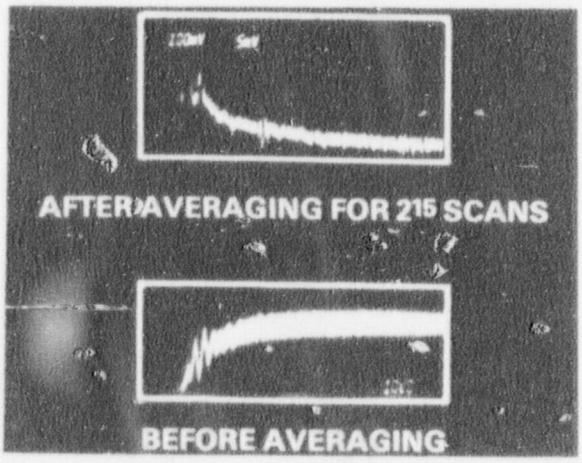

Figure 1. Demonstration of sensitivity-enhancement capability of signal averager: (a) Backwall reflection from 5 cm thick polymethylmethacrylate/stainless steel fiber composite, (b) Backwall reflection from 13 mm thick teflon, (c) Reflection from 4 mm hole, 6.5 cm deep, in austenitic stainless steel.

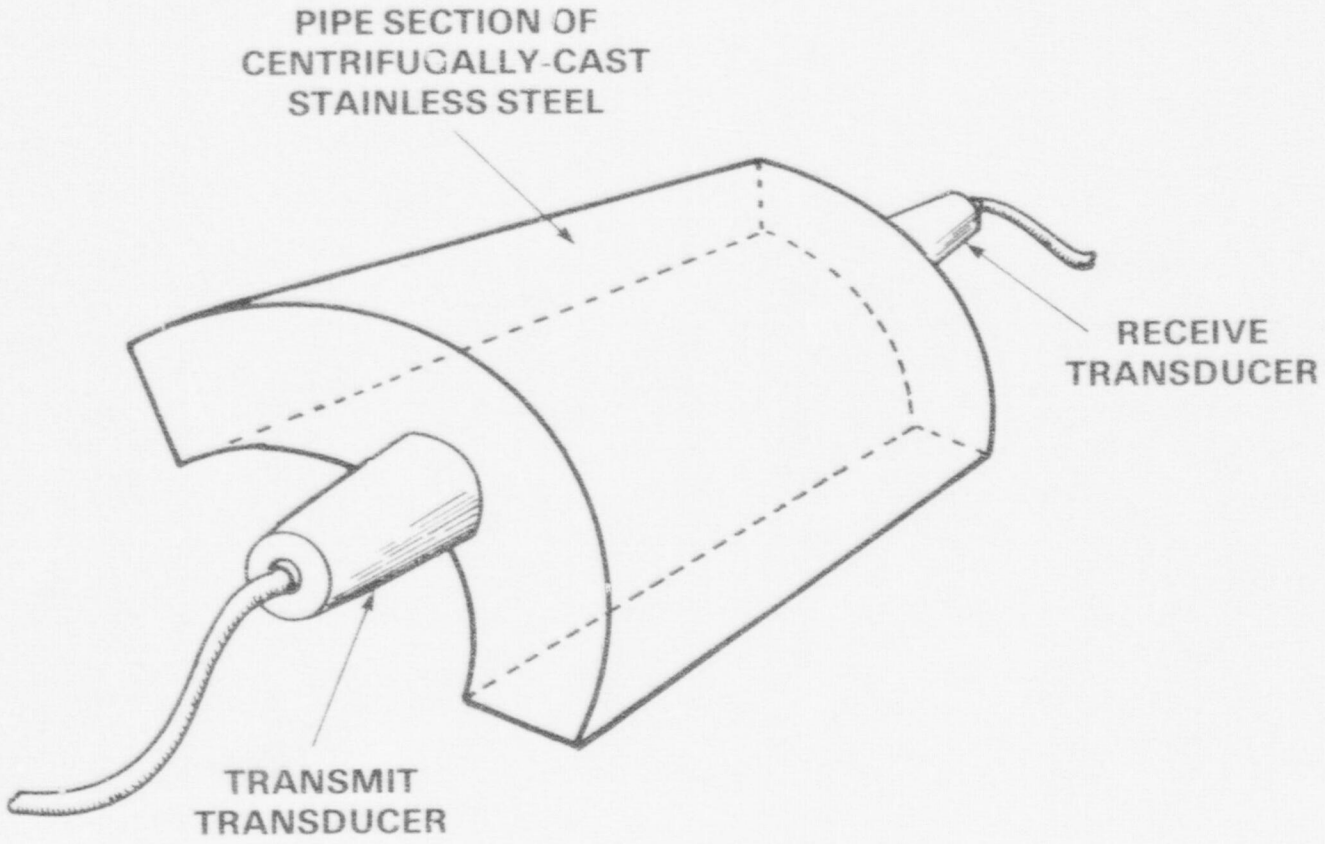
PIPE SECTION OF
CENTRIFUGALLY-CAST
STAINLESS STEEL
RECEIVE
TRANSDUCER
TRANSMIT
TRANSDUCER

Figure 3a shows the output of the receive transducer without averaging. The small signal, approximately midway across the trace, is the transmitted signal; its peak is seen to be just above the random noise of the ultrasonic receiver. Figure 3b shows the output after signal averaging. Up to the first arrival of the ultrasonic signal at the receive transducer, the system is looking at purely electronic noise and thus averages it out relative to the transmitted signal. However, after the first arrival, which corresponds to the most direct path for the ultrasonic signal, additional signals appear which arise from grain scattering. Since these scattering signals are stationary in time, they do not get averaged out. Indeed, the signal averager enhances these signals, along with the first arrival signal, relative to the random noise. In the case shown in the figure, the amplitude of the first arrival signal is just barely above the grain-scattering signal.

The above example illustrates the advantages and limitations of temporal signal averaging. If the signal were random-noise limited, e.g., if the signal were below the electronic noise due to penetration of a thick section of steel, signal averaging would be effective. However, temporal signal averaging will not average out stationary clutter due to grain scattering. Hence, in certain regions of the steel, where the clutter was particularly severe, no backscattered signal could be observed.

In contrast to temporal averaging, spatial averaging has been reported (1) to be effective in reducing "structural" noise. In this approach, the transducer is moved in a continuous and uniform fashion across the material. The grain noise recorded during each pulse-to-pulse interval is thus randomized in time and can be averaged out. Experiments along this line using our high-speed averager are planned for FY-79.

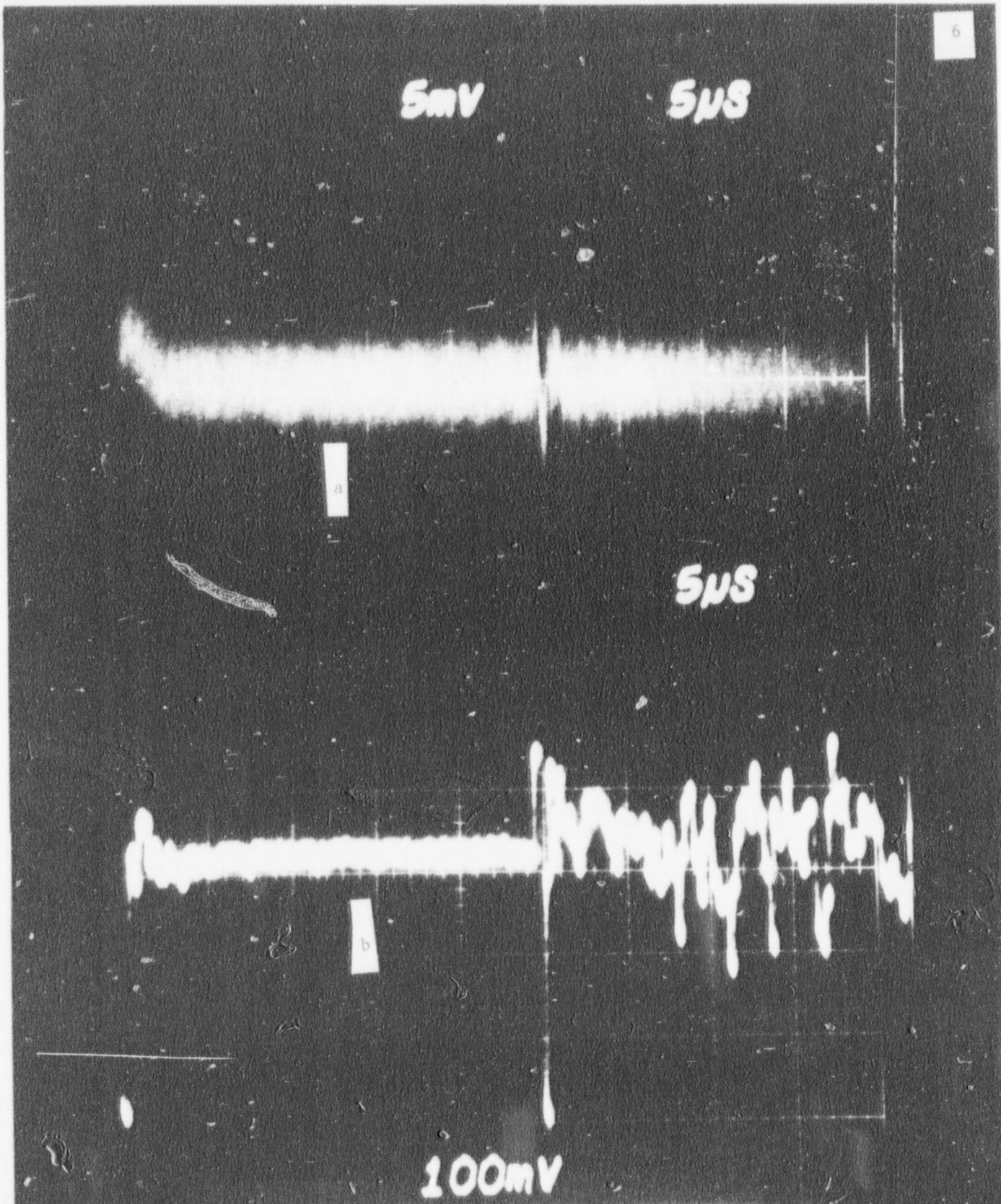

Figure 3. Output signal of receive transducer in transmission experiment (a) before and (b) after averaging.

2. Pulse Compression

A. Introduction

Pulse compression techniques have their greatest utility in echo ranging systems in which peak power output sets a limit on sensitivity. A short pulse is expanded into a "chirp", so that it is time-tagged. Because the pulse is longer, the total energy of the pulse (time integral of power) is increased. The returning echo is recompressed by means of a frequency-dispersive filter that reverses the expansion process. Because the pulse is higher in energy, sensitivity with respect to random electronic noise is improved in proportion to the increase in energy.

The most extensive use of chirp compression has been in radar systems. In such systems, the bandwidth is typically 0.1% of the operating frequency. As a result, the beam pattern and sensitivity of the antenna, the attenuation in the air, and the phase dispersion of the air, are all practically uniform over the system bandwidth.

In contrast, ultrasound systems must operate at low frequencies because of absorption and scattering of the sound waves in the medium. In order to get adequate range resolution, systems typically must employ bandwidths comparable to the operating frequency itself (in our system the chirp began at 3 MHz and ended at 12 MHz).

The result of this wide bandwidth is nonuniform response. The transducer pattern and sensitivity change with frequency, and the absorptivity and scattering may be much different at the minimum and maximum operating frequencies. These effects can be compensated for to some extent by appropriate changes in the driving signal as the transmitted pulse is being generated.

In the first year of the program, an 8:1 pulse compression ratio was achieved. This was increased in the current year to 30:1, with a compressed pulse width of 0.2 μs. This pulse width corresponds to a range resolution of ~0.6 mm (longitudinal waves) and 0.3 mm (shear waves) in steel.

B. System Design

The pulse compression device was designed using standard elements whenever possible. A block diagram is shown in Figure 4.

A free-running multivibrator triggers the firing sequence at a repetition rate of about 2 KHz. A voltage-controlled oscillator is enabled and a swept control voltage causes the oscillator to put out a linear sweep. Optimizing adjustments on this sweep include starting frequency, sweep rate, and linearity.

The swept RF output signal is amplitude-modulated in order to offset the frequency-dependent effects cited earlier. Since the output frequency is time-dependent, one may compensate for attenuation simply by increasing the amplitude of the output envelope during the time strongly-attenuated frequencies are being transmitted. It is thus much easier to achieve a controlled frequency response characteristic for the chirp device than with conventional impulse-type systems.

A transmitted envelope which is highly peaked results in reduced system bandwidth and correspondingly broader recompressed pulses. Too broad an envelope narrows the recompressed pulses at the expense of introducing low amplitude sidelobes (15-30 dB down) before and after the main response. We chose a round-shouldered response that narrowed the peak without introducing objectionable sidelobes.

The frequency of the driving signal was swept from 3 MHz to 12 MHz in a period of 5.5 μs. This modulated signal was fed through a commercial broadband RF amplifier and then through crossed diodes into a transducer. The transducer was coupled to a 2.5 cm thick aluminum plate in order to observe the backwall reflection. The reflected signal was preamplified in a commercial ultrasound unit.

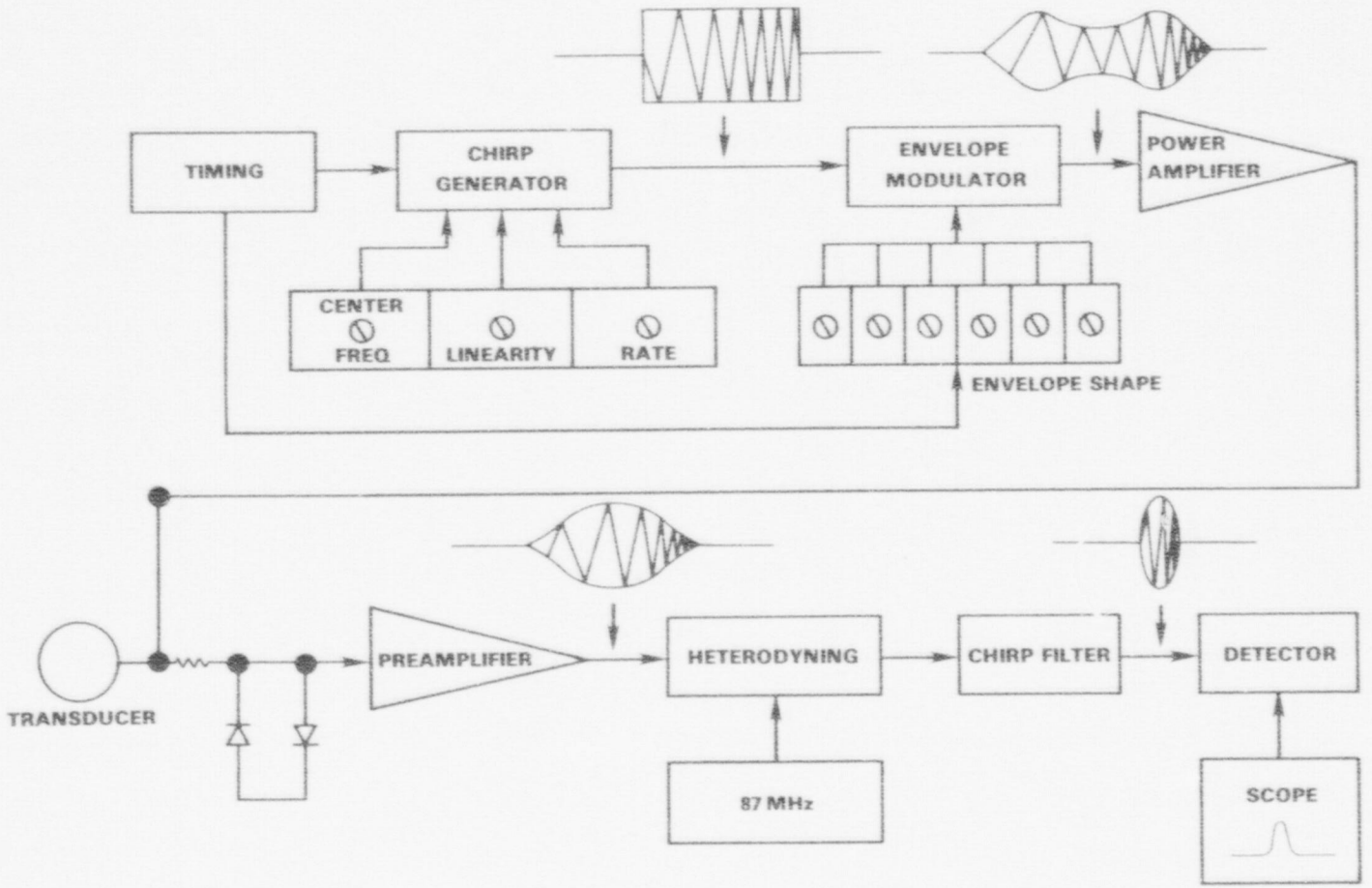

Figure 4. Block diagram of pulse compression system.

Our chirp filter, provided us by Hughes Research Labs., had a third overtone center frequency of 96 MHz, with an 8 MHz bandwidth. It was therefore necessary to heterodyne our 9 MHz ultrasound signal to 96 MHz using a doubly-balanced mixer. The heterodyned signal passed through the filter to an amplifier and detector, from which the detected A-scan signals were sent to an oscilloscope for viewing.

The resulting waveforms are shown in Figure 5. A pulse compression ratio of 30:1 is seen to have been achieved. This circuit would thus allow a corresponding increase in ultrasonic power transmitted to a material. Furthermore, because of the apodization of the transmitted signal to compensate for frequency-dependent attenuation, higher resolution is potentially obtainable with the chirp system than with a conventional impulse system.

3. Dynamic Focusing

Dynamic focusing not only improves sensitivity but also improves lateral resolution, and, as is demonstrated below, discriminates against coherent background caused by grain scattering. A unique dynamically-focused annular array suitable for contact B-scanning has been constructed under this program. The array approximates a constant f-number lens by dynamically expanding the lens aperture as the focal length increases. This approach minimizes the total number of discrete delay elements as well as the rate at which they must be switched without sacrificing resolution. An additional aspect of the expanding aperture design is that the outer annuli are of constant width, permitting a large active area and hence, high sensitivity.

A. Basic Concepts

The acoustic field distribution, U(r), in the focal plane of a lens of radius, a, with a uniformly weighted aperture is:

$$U(r) = \frac{2 J_1(\frac{2\pi ar}{\lambda z})}{(\frac{2\pi ar}{\lambda z})} \qquad (1)$$

(a)

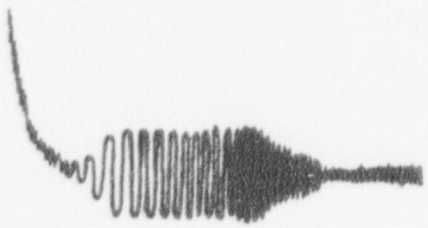

EXPANDED PULSE

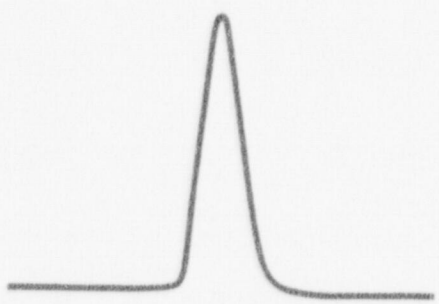

(b)

COMPRESSED PULSE

Figure 5. Demonstration of pulse compression capability of chirp radar system: (a) preamplified normal echo from near of a 1" thick aluminum block, (b) the same signal following compression and detection. A 6 μs pulse is compressed to a halfwidth of 0.2 μs.

where J_1 is the first order Bessel function, z is the focal length, λ the wavelength of sound, and r the distance from the axis of the lens.

The first order zero of this two-dimensional diffraction pattern occurs at

$$r_o = 1.22\ \lambda z/2a \qquad (2)$$

and is considered the minimum separation at which two point sources can be resolved. The beam width at half maximum for a single lens is

$$\approx 1.4\ \lambda z/2a,$$

and for a lens used in both transmit and receive

$$\approx 1.0\ \lambda z/2a.$$

The resolution parameter z/2a (focal distance/aperature) is known as the f-number.

An annular-array transducer consists of a central disc and a number of concentric annuli. With appropriate signal processing, this transducer can simulate a lens, although the resolution would be somewhat degraded from that of the uniformly-weighted aperture described above. This simulation is achieved by inserting appropriate electronic delays in both the transmit and receive circuitry of each annulus so the energy arrives at and is received from the focal region in phase. By periodically switching in different sets of delay elements, a dynamic focus, i.e., a focus which travels at half the speed of sound, can be generated in receive. For a fixed array size, the resolution would degrade in inverse proportion to the focal length (Eq. 2).

In the design reported here, the lens aperture is dynamically increased as the focal length increases so as to maintain roughly the same resolving power, or f-number, throughout the range of interest.

While the physical size of the transducer array must be fixed, the active aperture can be expanded electronically by sequentially inserting annuli of larger diameter into the circuit until the maximum physical diameter is reached.

This "expanding aperture" approach has significant advantages over conventional fixed-aperture designs in terms of minimizing hardware requirements. In particular, it significantly reduces the maximum time delays and switching speeds required to implement dynamic focusing.

A schematic diagram of the operation of the expanding aperture array system is shown in Figure 6. Because of physical limitations, the maximum attainable aperture is less than the maximum focal length, so that a constant f-number is not actually achieved.

In a wide bandwidth imaging system, a time delay must be inserted between the signals from the various annuli to account for the differences in path length from the focus to different points on the transducer face. For example, the time delay required between the central element of the array and a ring of radius R_n is:

$$t = \frac{(R_n^2 + z^2)^{\frac{1}{2}} - z}{c} \approx \frac{R_n^2}{2zc} \qquad (3)$$

where z is the focal length and c is the velocity of sound in the medium. The maximum time delay is given by

$$t_{max} = R_{max}^2/2z_o c \qquad (3a)$$

where R_{max} is the radius of the largest active annulus (and is therefore equal to 1/2 the aperture) and z_o is the minimum focal length. By keeping R_{max} small at the minimum focal point, the expanding aperture mode of operation reduces the maximum time delay which is required.

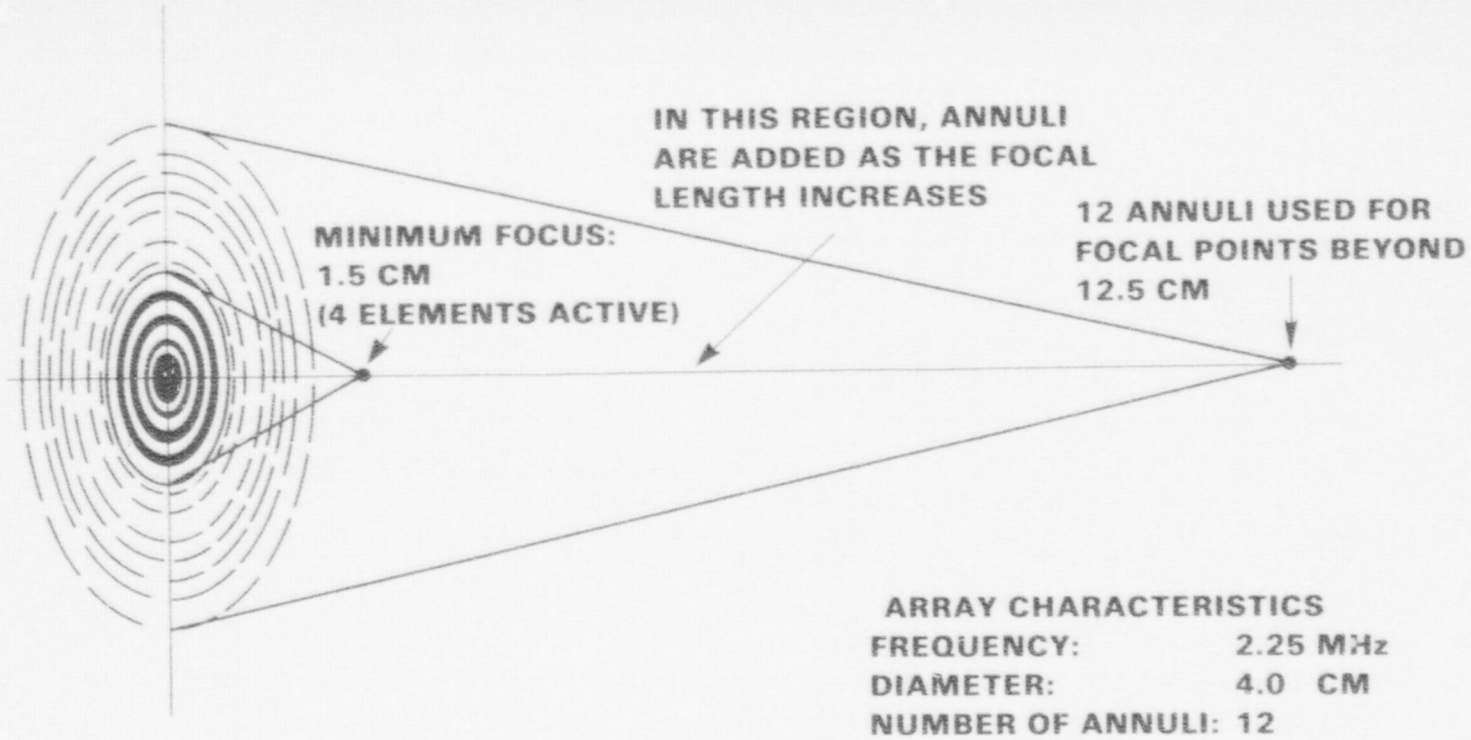

Figure 6. Principles and schematic diagram of expanding aperture annular array used for dynamic focusing on receive.

At a single frequency $\omega = 2\pi f$, the difference in phase for energy propagating from the focal point z_o to the central disc and to an annulus of radius R_n is given by ϕ, where:

$$\phi = \frac{\omega R_n^2}{2zc} \tag{4}$$

The maximum rate of change of this phase difference is:

$$\left(\frac{\partial \phi}{dt}\right)_{max} = \left(\frac{\partial \phi}{\partial z}\ \frac{dz}{dt}\right)_{max} = \frac{-\omega R_{max}^2}{4\ z_o^2} \quad . \tag{5}$$

For dynamic focusing, the lens must be refocused every $\pi/2$ phase shift by inserting different combinations of delay elements. The maximum switching frequency, $(f_s)_{max}$, is given by:

$$(f_s)_{max} = \left(\frac{\partial \phi}{\partial t}\right)_{max} /(\pi/2) = \frac{\omega\ R_{max}^2}{2\pi z_o^2} \tag{6}$$

With fixed-aperture dynamic systems, a large initial f-number, and hence large f_s, is required in order to obtain an acceptable f-number at the largest z values. The expanding aperture approach, or the other hand, allows operation at a smaller initial f-number and hence smaller initial f_s. Switching rate requirements are kept well below the signal frequency throughout the entire focal zone.

The operation of our array during a single A-scan can be understood by reference to Figure 7. The delay line consists of 10 taps, at 100 ns, intervals giving a maximum delay of 1 μs. At the beginning of the A-scan only the central five elements of the array are activated so as to focus at the minimum focal point, z_o = 1.5 cm: The annuli R_1-R_5 are connected to taps 1,1, 3,5, and 10, respectively. As the focal length increases during the A-scan, these delay elements are switched and another annulus activated whenever the time delay between it and the central element becomes less than a microsecond. For focal lengths greater than 10 cm, the entire array of 12 rings is active.

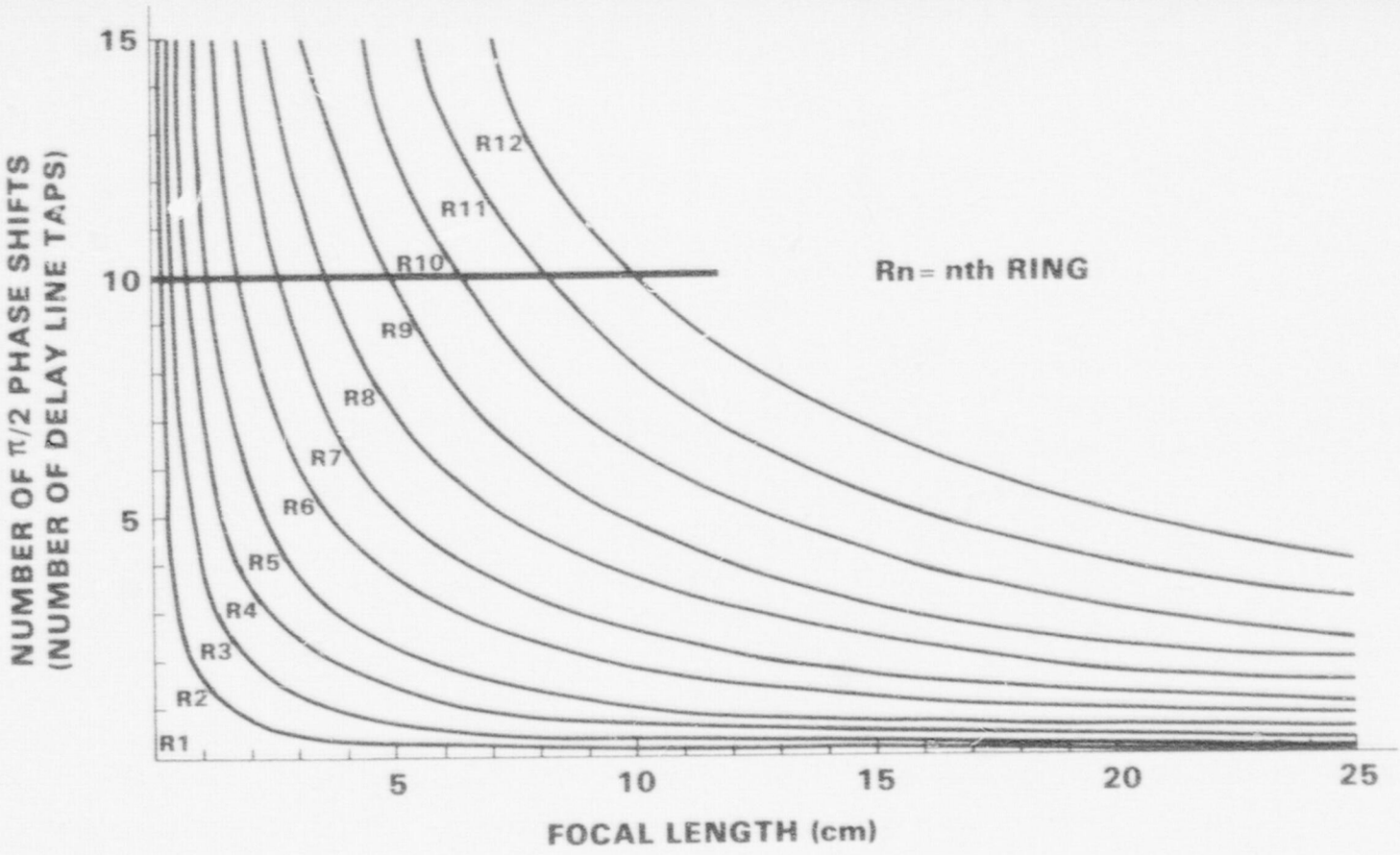

Figure 7. Plot of delay vs. focal position for each of the 12 elements of the annular array.

In addition to minimizing hardware requirements for dynamic focusing, the expanding aperture approach also increases the sensitivity of the transducer. The maximum width of an annulus is determined by requiring the phase shift across the annulus be less than $\pi/2$ for a signal from the nearest focal point for which the element is activated. The expanding aperture approach results in an equal width criterion as compared to an equal area criterion for a Fresnel Zone plate design. Since the area of an annulus in our design increases with its radius, the array will have a larger active area, thus providing more power on transmit and greater sensitivity on receive.

B. Dynamic Focusing Electronics

Figure 8 is a block diagram of the delay line network used to provide the relative time delays required for dynamic focusing on receive. The output of each array element is amplified by either a linear or logarithmic amplifier and is multiplexed into a single tapped lumped-constant delay line. The output of the delay line is the coherent sum of the signals driving the individual taps. The delay line is 1 μs long, has ten taps and a bandwidth of 10 MHz. The circuit for multiplexing the R.F. signal from an array element into the delay line is shown in Figure 9.

Each array element drives a cascode amplifier with ten output stages. The base of transistors $S_1 \ldots S_n$ are connected to the output of a binary decoder which activates one of the ten output stages. Thus, only one common base stage is turned on at a time, and a single transistor serves as the analog switch. Point A_1 is the common point for the outputs of all stages connected to tap #1. For this system with twelve elements, the high impedance outputs of twelve cascode amplifiers are thus connected to each point A_1. Transistors B_1, always on, isolate the delay line from the output stages of the cascode amplifiers.

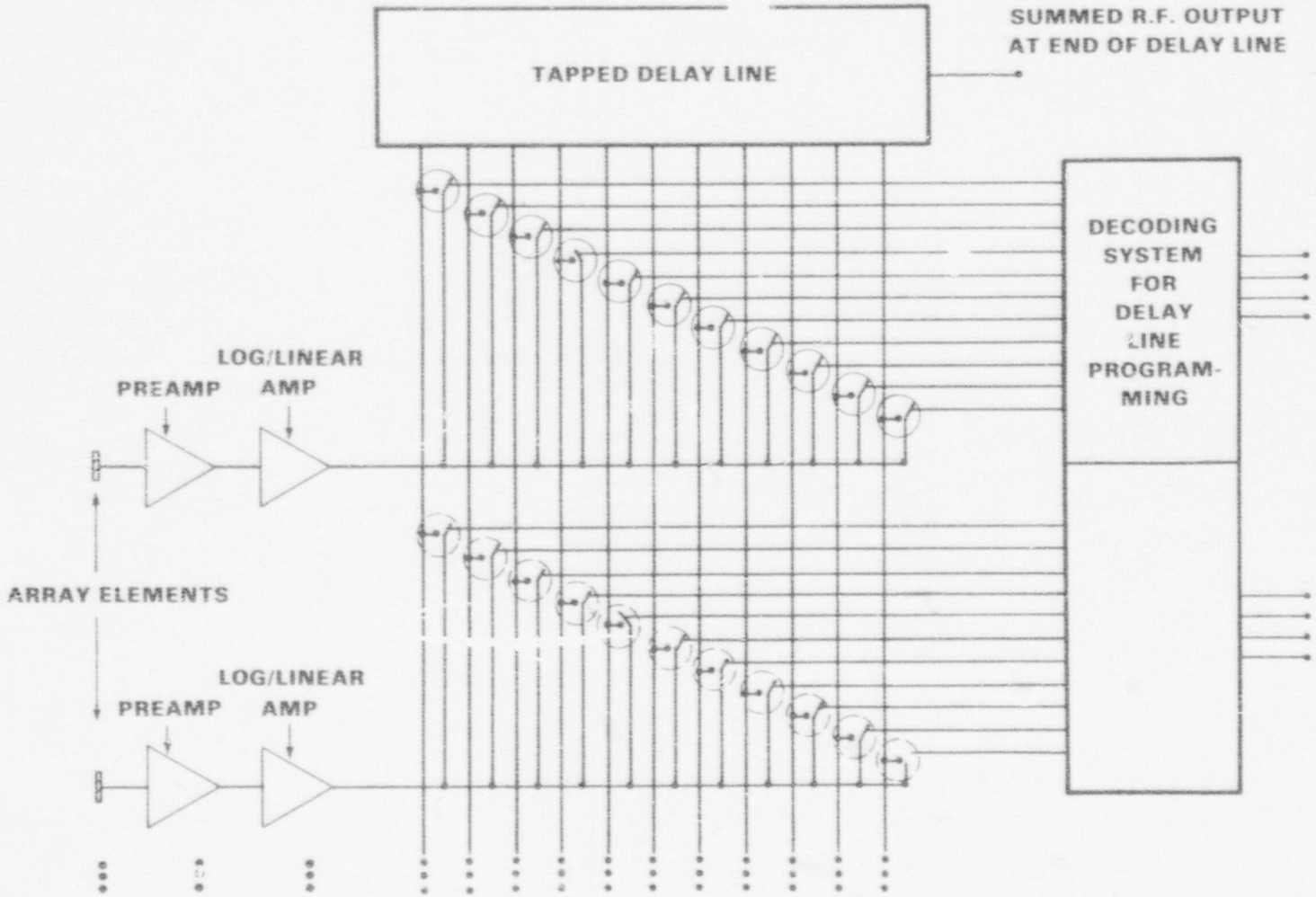

Figure 8. Schematic diagram of circuit for focusing on receive.

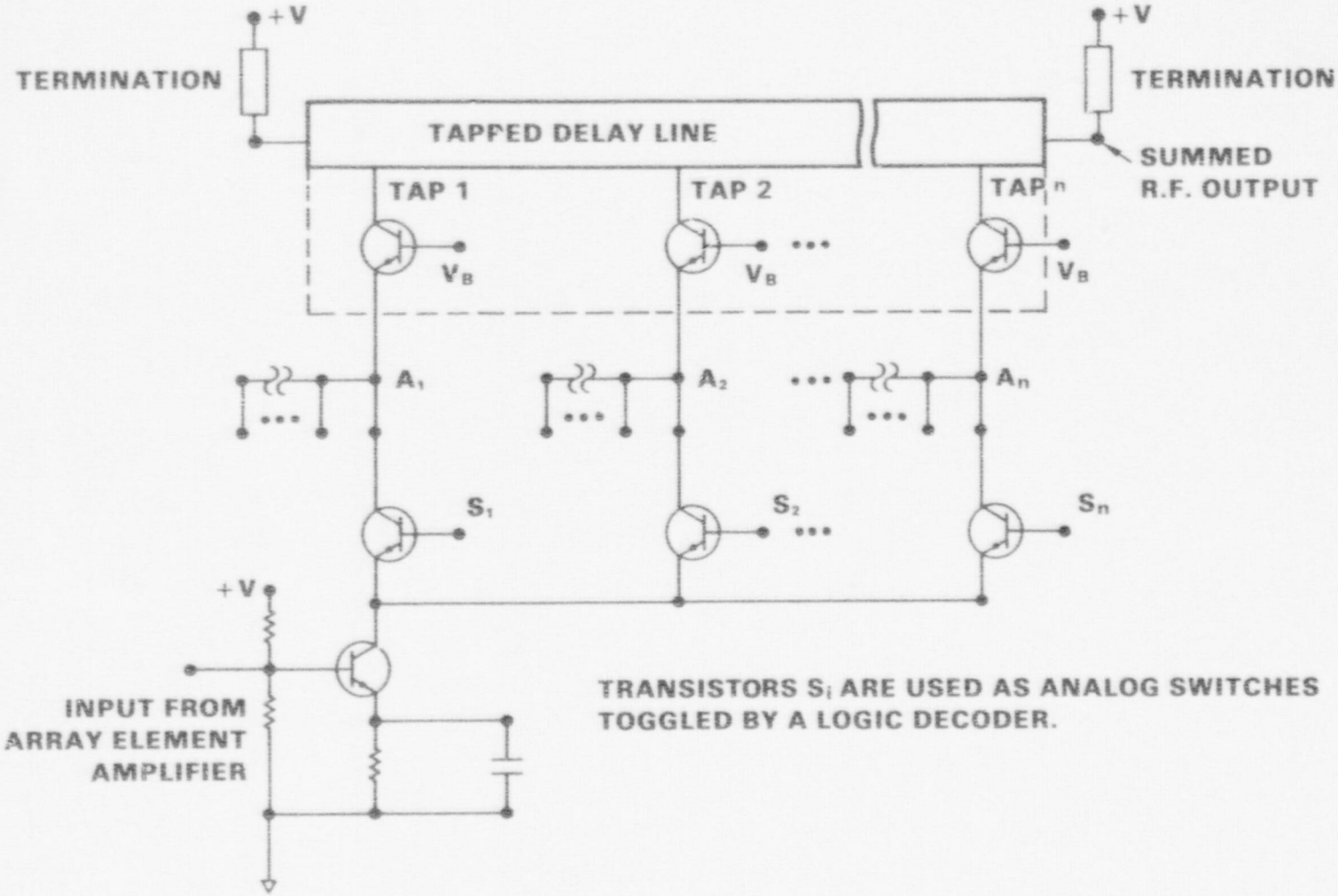

Figure 9. Cascode Amplifier - Multiplexer Circuit. Transistors S_1, S_2 . . . , are used as analog switches toggled by a logic decoder.

The switching sequence that drives the decoders is stored in a ROM that is clocked with a period of approximately 3 μs. When a single tapped delay line is used, the number of analog switches required is N x M, where N is the number of array elements and M is the number of delay increments. Since each array element drives only one tap at a time, the number of binary control bits required is approximately N $\log_2$M. In contrast, a system that uses a separate delay line for each array element, as is commonly done, requires approximately N $\log_2$ M switching terminals, delay elements, and control bits. The simplicity of a single delay line in our system is gained at the price of a larger number of analog switching terminals. The single transistor switching stage, combined with the expanding lens approach, makes this a viable alternative.

C. Focus on Transmit

With the dynamically-focused annular array used as a receiver, only the echoes from reflectors on the axis will sum coherently. Azimuthal resolution will be further improved if the transmitted power is concentrated along the axis. This can be done by transmitting either a spherical wavefront producing a point focus, with sufficient depth of field, or a conical wavefront producing a line focus. The focus on transmit is generally implemented by a set of discrete time delays that determine the relative firing time of the array elements. One set of such time delays is required for each focal zone. While several overlapping focal zones should be sufficient for most imaging systems, the technique we describe here provides a continuously-variable focus on transmit. This scheme has potential application to beam steering and focusing arrays other than the annular design discussed here.

Figure 10 is a block diagram of the circuit for generating the focal zone on transmit. A comparator is used to trigger the high-voltage pulser of each array element. The wavefront curvature is coded in the resistor chain which is calculated so that the voltage difference between

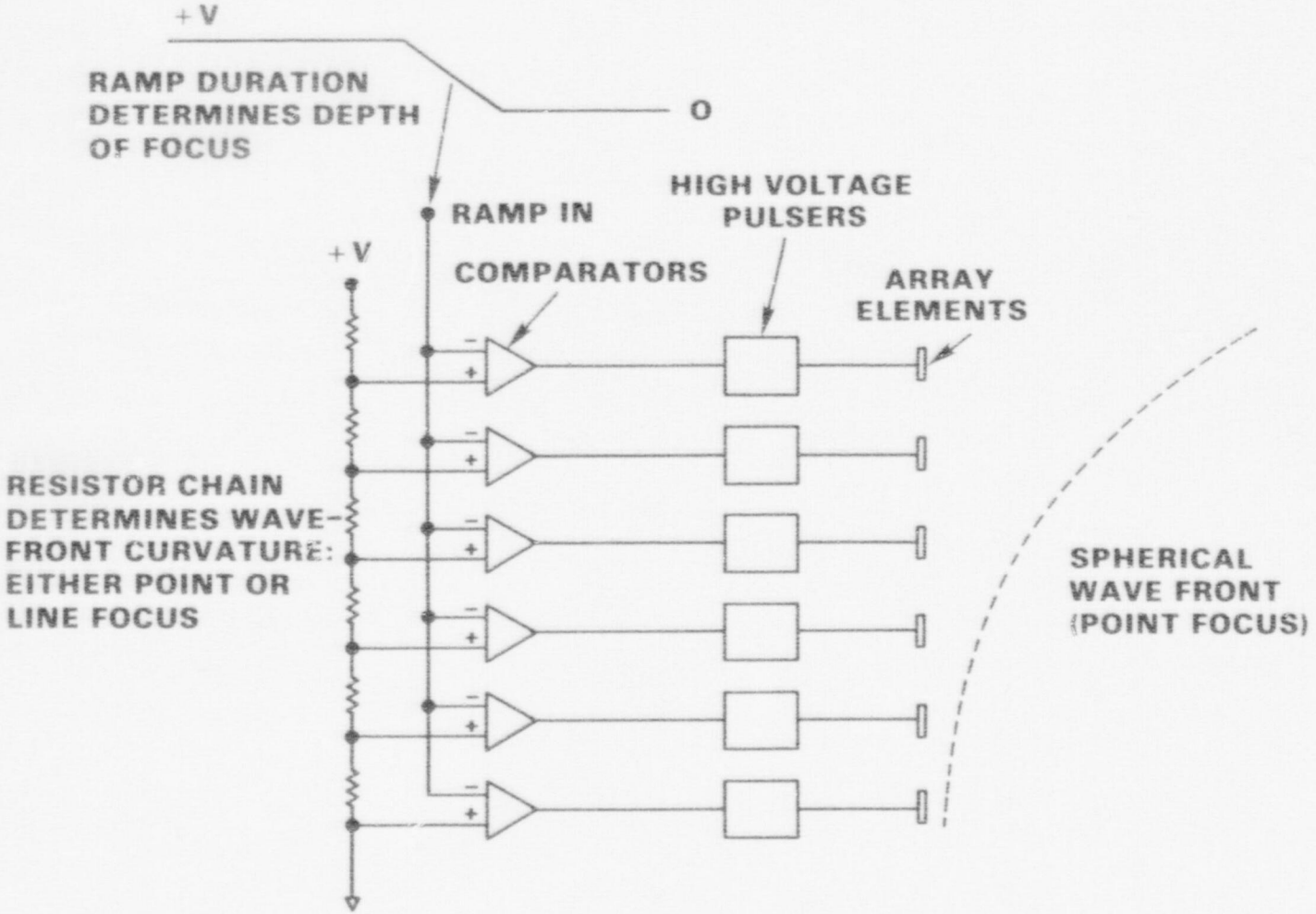

Figure 10. Schematic diagram of circuit for focusing on transmit.

taps "i" and "j" is proportional to the difference in radii for a line focus, or the difference in the square of the radii for a point focus.

$$V_1 - V_j \propto \begin{cases} R_i^2 - R_j^2 & \text{Point focus} \\ R_i - R_j & \text{Line focus} \end{cases} \qquad (7)$$

The i^{th} tap on the resistor chain provides the voltage imput of the i^{th} comparator which fires the high voltage pulser of the corresponding array element. The second terminal of each comparator is driven by the voltage ramp.

For a point focus, the time difference between the firing of elements "i" and "j" is given by:

$$t_i - t_j = \frac{V_i - V_j}{K} = \frac{R_i^2 - R_j^2}{2zc} \qquad (8)$$

where $K = dV/dt$ is the ramp rate. Thus, when $(V_i - V_j)$ is proportional to $(R_i^2 - R_j^2)$, the ramp rate K is proportional to the focal length. The half width and sidelobe level of the transmitted beam in the focal plane are similar to that measured when the same array is focused on receive.

The transmit focusing technique can be used, independent of the dynamically-focused receiver, to produce an electronically-variable focusing system consisting of a single annulus as a receiver and the full array as the focused transmitter. The delay line as well as the dynamic-focus electronics are thus eliminated. This design is characterized by trivial electronic hardware costs and would make a very practical system for field use.

The focusing properties of this design may be derived from the product of the individual field patterns of the transmitter and receiver in the focal plane. At a single frequency, the field distribution, U(r), of a thin annulus is concentrated along the axis and has the form:

$$U(r) = J_o\left(\frac{2\pi ar}{z}\right) \qquad (9)$$

where J_0 is the zeroth-order Bessel function. While the main lobe of this distribution is narrow, the sidelobes are large and decrease slowly with off-axis distance r. However, the product of this pattern in receive with that of a full aperture in transmit, or, in this case, a large number of annuli, results in a field pattern which is very acceptable for acoustical imaging. In the wide bandwidth limit in which a pulsed system operates, an even better field pattern is generated. While the switching and A-D conversion speeds required to implement dynamic focusing on receive become more difficult to implement as the operating frequency is increased, the only limitation on this simpler type of electronic focusing is the response of the transducer array. Such systems may thus be very useful in applying electronically-variable focusing at high frequencies to nondestructive testing.

D. Beam Plots

Beam plots of the dynamically-focused annular array, measured in water at 2.5 MHz, are shown in Figure 11. The half-width at the focus ranges from 1.5 mm at a 3.0 cm focus to 3.2 mm at 15 cm. These values are in close agreement with theoretical predictions. Switching noise and side-lobe levels are approximately 40 dB down. Figure 12 is a plot made with the imaging system consisting of the full array on transmit and a single element on receive. The resolution is seen to be comparable to that achieved with the full array.

E. Experimental Results

Annular array focusing using both all annuli (Mode I) and only the outer annulus (Mode II) during the receive phase of operation was demonstrated on several samples of interest to nuclear reactor monitoring. Figures 13-15 show results of these measurements, for natural weld flaws in a pressure vessel steel (Figure 13) and a steel pipe (Figure 14), and for a backwall reflection from a two-inch thick wall of centrifugally-cast

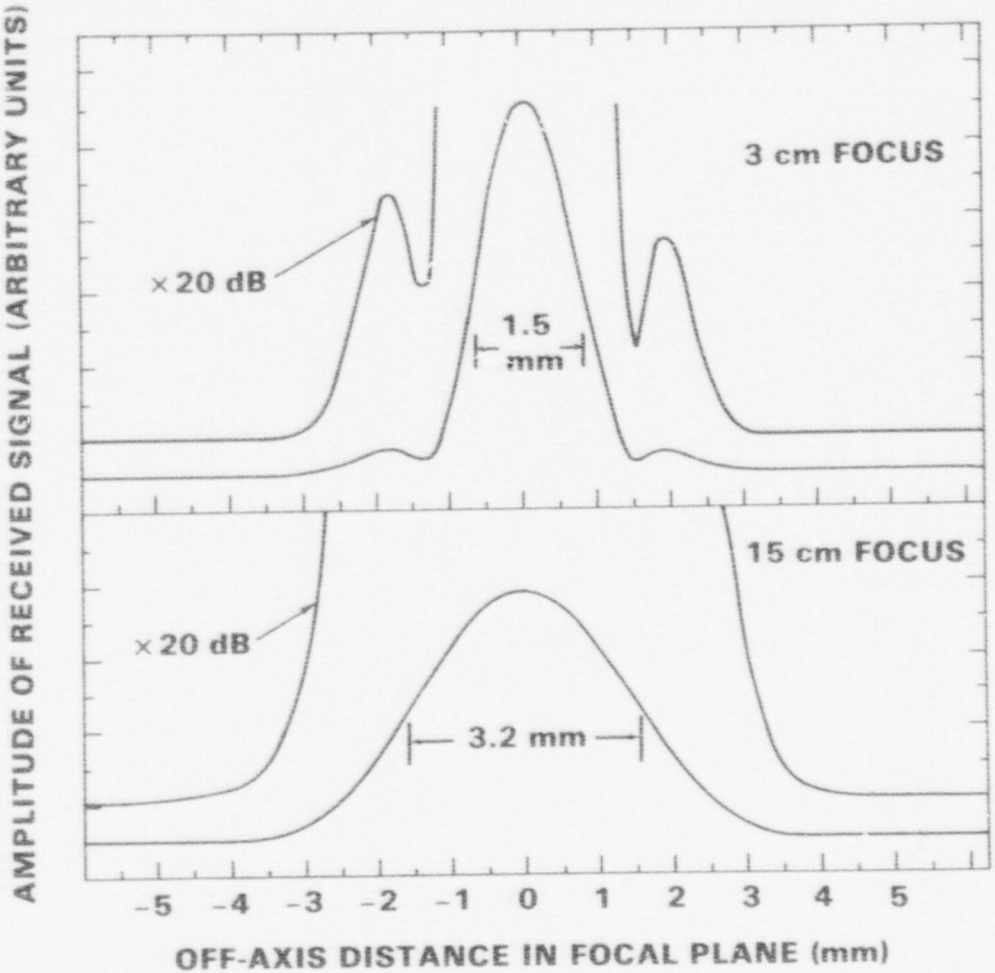

Figure 11. Beamplots for the annular array system at (a) 3.0 cm and (b) 15.0 cm focal points in water.

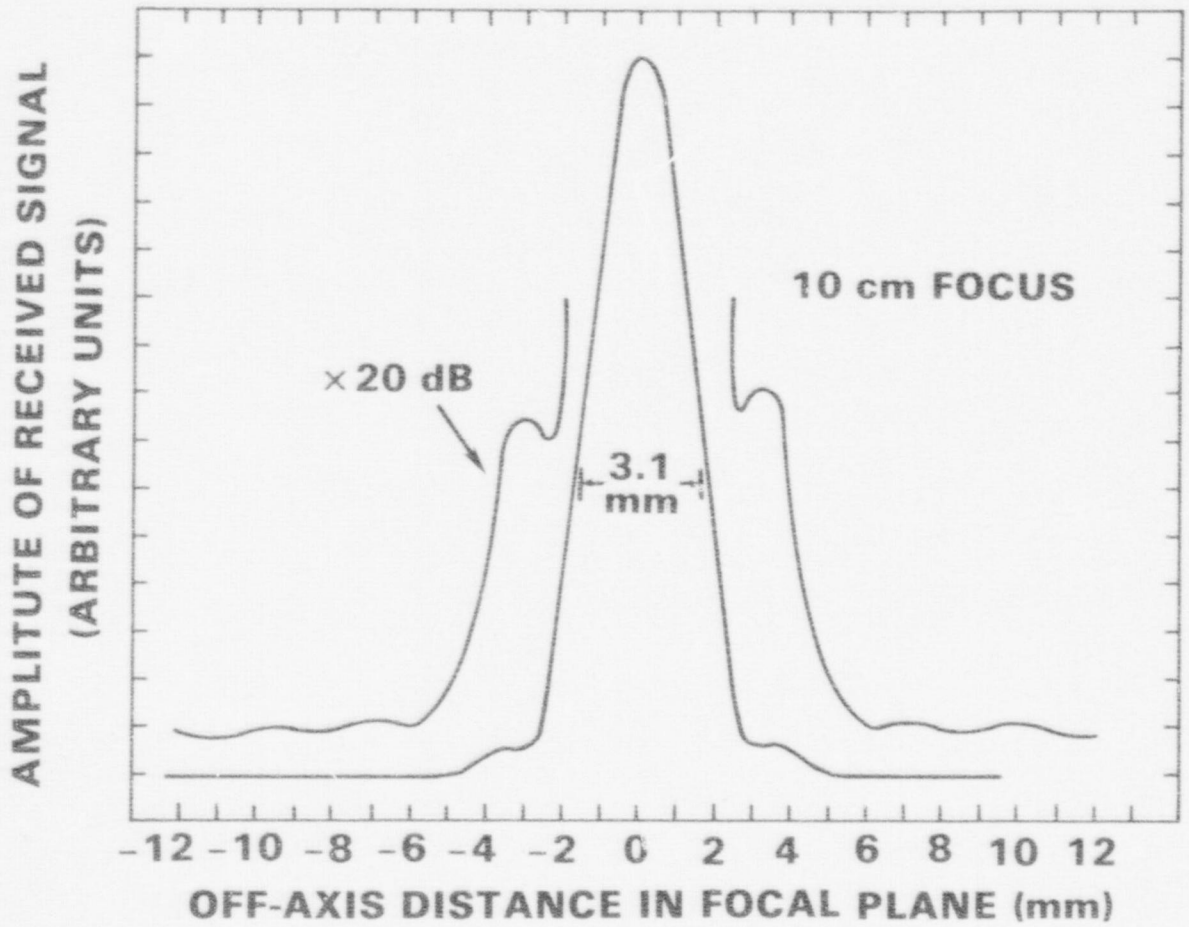

Figure 12. Beam plot at 10 cm focus, with the full array transmitting and a single annulus as the receiver. The sidelobe plot is shown with a 20 dB increase in gain.

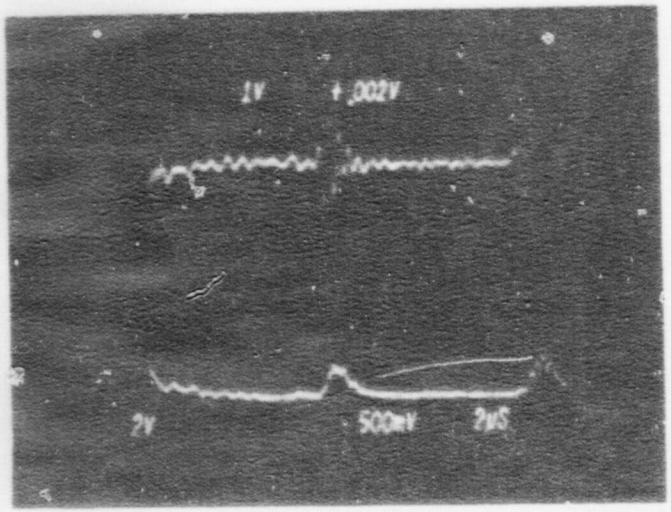

(a) 1 2 3

REFLECTION FROM NATURAL FLAW IN PRESSURE VESSEL STEEL WELD

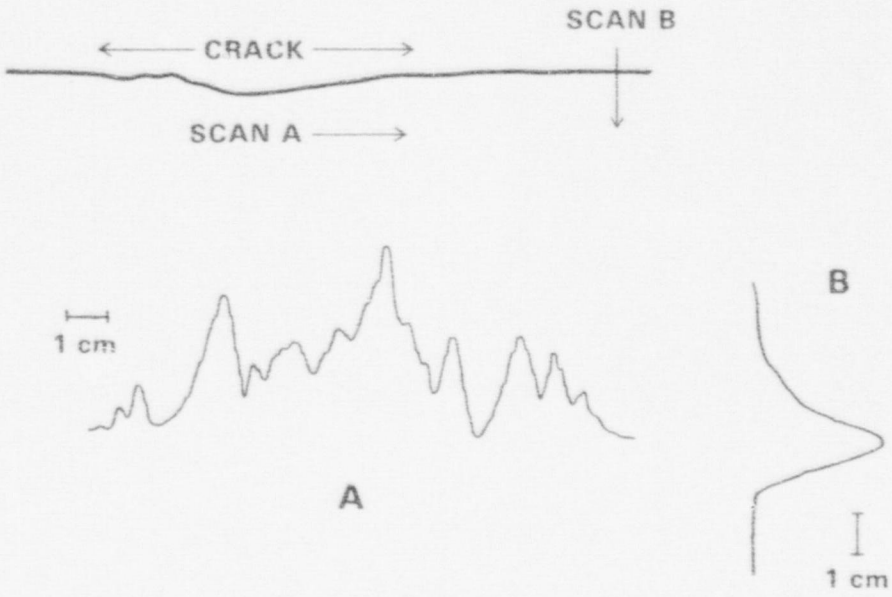

(b)

Figure 13. (a) Front wall (1), flaw (2), and backwall (3), reflection from a pressure vessel steel weld. Upper and lower photos display r.f. and video signals from an A-scan at position z_o. (b) Linear scan of the same weld in two orthogonal directions showing the amplitude of the reflected signal versus distance. The x-axis plot is comparable to the bandwidth implying that the flaw is a thin crack. The z-axis plot shows the length of the crack.

(a)

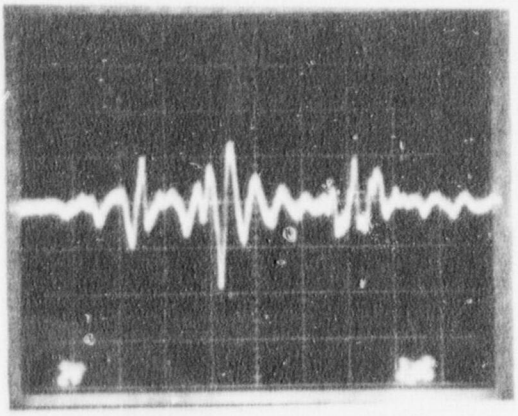

1 2 3

(b)

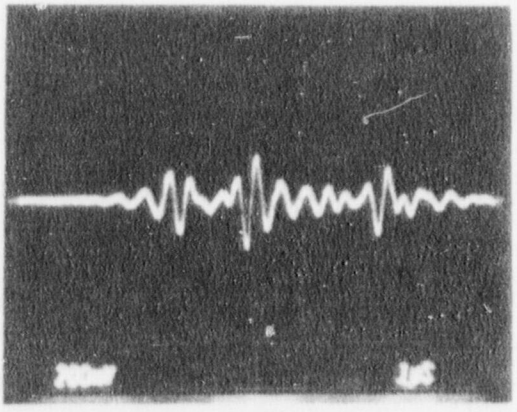

1 2 3

(c)

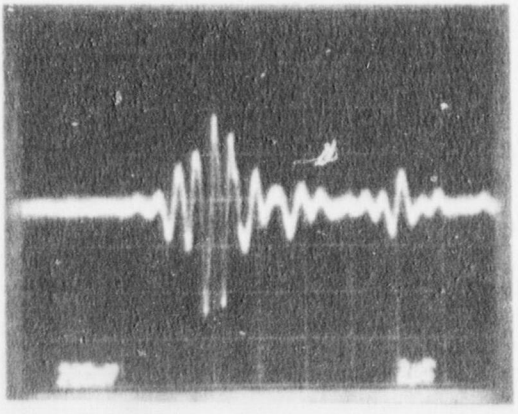

1 2 3

Figure 14. A scans from weld section in 14" diameter x 7/16" wall stainless steel pipe showing reflections from front wall (1), flaw (2), and backwall (3): a) Mode I focusing, b) Mode II focusing, c) Unfocused transducer.

stainless steel pipe (Figure 15). Note the high resolution achieved with the focused system, even with the Mode II approach, compared with the non-focused system. The nonfocused transducer system cannot even detect the back-wall reflection from the centrifugally-cast tubing. This is due primarily to the coherent background noise arising from grain scattering, with the increased attenuation due to the scattering playing a secondary role. The annular-array focusing system not only increases the signal-to-random noise ratio and hence overcomes the attenuation due to scattering, but, more importantly, reduces the coherent noise since fewer grains are observed within the small focal region.

4. Transducer Matching and High-Power Insonification

Transducer matching increases the power transmitted to and received from the region of interest. Because of the commercial availability of matched transducers, we have decided to purchase our annular array transducer already matched rather than attempt to fabricate our own matching layers.

Sensitivity enhancement by high-power insonification is ultimately limited by the power handling capability of the transducer. As the power is increased, a dangerous feedback mechanism comes into play, where the increased power dissipated in the transducer raises its temperature, thereby increasing the loss tangent, which, in turn, raises the temperature further. Estimates from work reported in the literature (2) indicate a power limit of the order of 0.5 kilowatts CW for a PZT transducer. In our own laboratory, we have transmitted 60 watts CW (the maximum power available to us) to a transducer immersed in water without any noticeable rise in temperature or change in the linearity of the output. CW rather than pulse insonification was employed in these tests because maximum power transmission in pulse echo devices can be obtained by use of expanded waveforms, such as in the chirp radar system which we have developed.

(a)

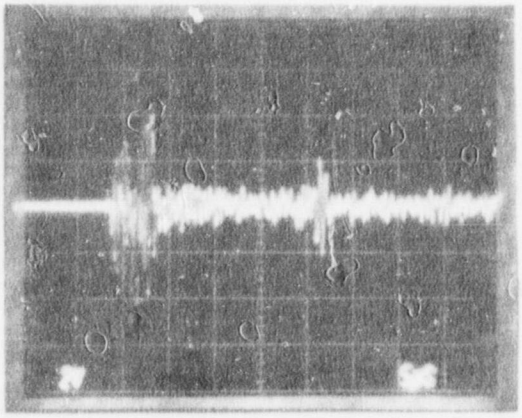

1

(b)

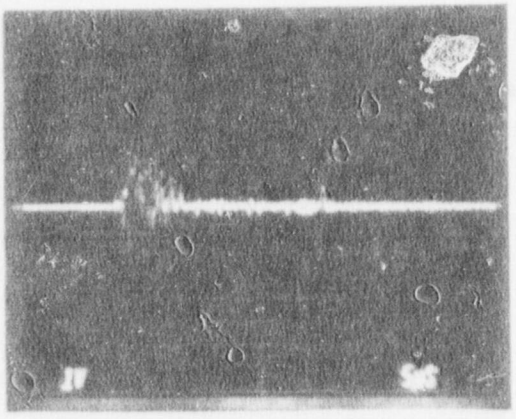

1

(c)

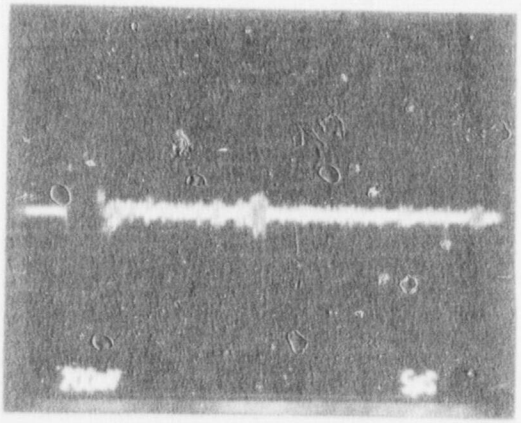

1

Figure 15. A-scans from section of 24" diameter x 2" wall centrifugally-cast stainless steel pipe. Backwall reflection is seen at location 1 in the case of (a) Mode I focusing and (b) Mode II focusing, but in absent when a nonfocused transducer (c) is used.

5. Integration of the Components of the Ultrasensitive Ultrasonic System

Signal averaging, transducer matching, pulse compression and high-power insonification can, in principle, be cascaded to form an ultrasonic system with a substantial increase in sensitivity over current devices. The combination of annular array focusing with a high power pulse compression system, however, would require separate high power amplifiers for each ring, and separate pulse compression filters for each ring in Mode I operation (all annuli active in receive) and one filter for Mode II (only outer annulus active in receive). The development of such an integrated system was not undertaken during the course of this study.

III. CONCLUSIONS AND PLANS FOR FUTURE RESEARCH

The highly sensitive system which we have developed should be capable of overcoming almost all random noise problems which are encountered in ultrasonic inspection of reactors. Other major needs in this field are improved lateral resolution and improved discrimination against coherent background due to grain scattering. As this study has shown, electronic focusing will significantly increase not only the signal-to-random noise ratio, but also the resolution and background-suppression capability of the system. However, because of the rigidity of the materials of interest and the large differences between the ultrasonic velocities in these materials and in typical transducer coupling media (water, oil, grease), image distortions will be produced when inspecting through surfaces which are not flat. Our efforts in the next two years will therefore concentrate on developing focusing and beam deflection schemes which, at reasonable cost, will allow inspection of hard materials. The use of shear waves will be investigated since it will provide a factor of two improvement over the use of longitudinal waves, due to its lower velocity. A theoretical analysis of array performance in the wideband case will be undertaken in order to

optimize array design for the focusing techniques under consideration. A two-dimensional stepper-motor driven scanner, with computer interface, will also be developed and used to generate B-scan images of flaws in materials. Finally, our high-speed signal averager will be used to spatially average out structural noise.

References

(1). I. N. Ermolov and B. P. Pilin, NDT International, pp. 275-280, 1976.

(2). D. Berlincourt, B. Jaffe, H. Jaffe and H. H. Krueger, IRE Trans. Ultrasonics Eng., pp. 1-6, 1960.

NRC FORM 335 (7-77)

U.S. NUCLEAR REGULATORY COMMISSION

BIBLIOGRAPHIC DATA SHEET

1. REPORT NUMBER (Assigned by DDC)
NUREG/CR-0460

4. TITLE AND SUBTITLE (Add Volume No., if appropriate)
Development of High-Sensitivity Ultrasonic Techniques for In-Service Inspection of Nuclear Reactors

2. (Leave blank)

3. RECIPIENT'S ACCESSION NO.

7. AUTHOR(S)
M. Linzer, D. Dietz, S. I. Parks

5. DATE REPORT COMPLETED
MONTH: May YEAR: 1978

9. PERFORMING ORGANIZATION NAME AND MAILING ADDRESS (Include Zip Code)
National Bureau of Standards
Institute for Materials Research
Department of Commerce
Washington, DC 20234

DATE REPORT ISSUED
MONTH: October YEAR: 1978

6. (Leave blank)

8. (Leave blank)

12. SPONSORING ORGANIZATION NAME AND MAILING ADDRESS (Include Zip Code)
Metallurgy & Materials Research Branch
Division of Reactor Safety Research
U.S.Nuclear Regulatory Commission
Washington, DC 20555

10. PROJECT/TASK/WORK UNIT NO.
B5680

11. CONTRACT NO.

13. TYPE OF REPORT
Annual

PERIOD COVERED (Inclusive dates)
10/1/76 - 9/30/77

15. SUPPLEMENTARY NOTES

14. (Leave blank)

16. ABSTRACT (200 words or less)

During the period covered by this report, an ultrasensitive untrasonic system, incorporating real-time signal averaging, pulse compression, dynamic focusing and transducer matching, has been developed. The system was shown to be capable of penetrating highly-attenuating material, such as austenitic steel, and of detecting reflections in the presence of strong background signals due to grain scattering.

17. KEY WORDS AND DOCUMENT ANALYSIS

17a. DESCRIPTORS

17b. IDENTIFIERS/OPEN-ENDED TERMS

18. AVAILABILITY STATEMENT
Unlimited

19. SECURITY CLASS (This report)
unclassified

21. NO. OF PAGES

20. SECURITY CLASS (This page)
Unclassified

22. PRICE
$

NRC FORM 335 (7-77)

120555003927 2 R5AN
US NRC
SECY PUBLIC DOCUMENT ROOM
BRANCH CHIEF
HST LOBBY
WASHINGTON DC 20555